Eur. Phys. J. E **5**, 605–614 (2001)

THE EUROPEAN PHYSICAL JOURNAL E

EDP Sciences

Diblock copolymer thin films: Parallel and perpendicular lamellar phases in the weak segregation limit

Y. Tsori and D. Andelman[a]

School of Physics and Astronomy, Raymond and Beverly Sackler Faculty of Exact Sciences, Tel Aviv University, 69978 Ramat Aviv, Israel

Received 10 May 2001 and Received in final form 6 July 2001

Abstract. We study morphologies of thin-film diblock copolymers between two flat and parallel walls. The study is restricted to the weak segregation regime below the order-disorder transition temperature. The deviation from perfect lamellar shape is calculated for phases which are perpendicular and parallel to the walls. We examine the undulations of the inter material dividing surface and its angle with the walls, and find that the deviation from its unperturbed position can be much larger than in the strong segregation case. Evaluating the weak segregation stability of the lamellar phases, it is shown that a surface interaction, which is quadratic in the monomer concentration, favors the perpendicular lamellar phase. In particular, the degeneracy between perpendicular and unfrustrated parallel lamellar phases for walls without a preferential adsorption is removed.

PACS. 61.25.Hq Macromolecular and polymer solutions; polymer melts; swelling – 61.41.+e Polymers, elastomers, and plastics – 68.55.-a Thin films structure and morphology

1 Introduction

Diblock copolymers (BCP) are made up of two chemically distinct chains covalently bonded together. The BCP system forms self assembled structures with length scales in the nanometer to micrometer range. On the level of mean-field theory, the bulk phase diagram is governed by two parameters: $f = N_A/N$, the fraction of the A-block in a chain of polymerization index $N = N_A + N_B$, and χN, where χ is the Flory parameter measuring the interaction between the two species, and is inversely proportional to the temperature [1–4].

For temperatures above the order-disorder transition (ODT) temperature the system is in the disordered phase. As the temperature is lowered, symmetric BCP melts ($f = \frac{1}{2}$) undergo a weak first order transition to a lamellar phase at $\chi > \chi_c$. As the degree of block asymmetry f is increased, $|f - \frac{1}{2}| > 0$, other phases of hexagonal and cubic spatial symmetries become stable [5–7].

The interfacial behavior of BCP melts has been the subject of experimental [8–11] and theoretical [12–20] investigations. In the former case the substrate is typically spin-coated by the BCP, and subsequently analyzed by small angle neutron and X-ray scattering or neutron reflectivity measurements. If the walls are neutral, *i.e.*, without preferential adsorption to one of the two blocks, thin films of lamellar diblock copolymers maintain their bulk periodicity d_0 by aligning perpendicular to the confining walls. Such long range ordering can be transferred by various techniques to a surface, creating a template useful in nanolithography [21]. In cases where the walls prefer one of the two blocks, the lamellae can reduce the interfacial interactions by aligning parallel to the walls, and change the lamellar periodicity from its bulk value d_0. Which of the two phases prevails (parallel or perpendicular) depends on the distance $2L$ between the two walls (film thickness), the strength of the wall interactions as well as the degree of segregation $N\chi$.

Numerical calculations of confined BCP have been performed using self-consistent field theory [15,16] and Monte-Carlo simulations [16,22]. Using these techniques, order parameter profiles and phase diagrams have been obtained. Previous analytic theories [22–24], while providing valuable qualitative results, have been sensitive to the specific choice of phenomenological coefficients, and this sensitivity leads to marked inaccuracies of the order parameter as compared to Monte-Carlo simulations [22].

In the present work we complement the numerical studies by introducing an alternative analytical method. In particular, we derive the deviation of the perpendicular and parallel lamellae from their bulk shape. In Section 2 we introduce a model free energy and derive the underlying equations. In Section 3 the shape of confined lamellae is investigated and found to be, in general, very different from the bulk shape. The energy of the perpendicular and parallel lamellae as a function of surface separation $2L$ as well as the stability diagram is discussed in Section 4.

[a] e-mail: andelman@post.tau.ac.il

2 Model

Close to the phase transition point (ODT) between the disordered and lamellar phases, the free energy of symmetric BCP melt is well described by the following Ginzburg-Landau expansion [7,17,18,25–27]:

$$\mathcal{F}_b = \int \left\{ \frac{1}{2}\tau\phi^2 + \frac{1}{2}h\left(\nabla^2\phi + q_0^2\phi\right)^2 + \frac{u}{4!}\phi^4 \right\} \mathrm{d}^3\mathbf{r}. \quad (1)$$

The bulk free energy $\mathcal{F}_b$ (in units of $k_\mathrm{B}T$) is given as a functional of the local order parameter $\phi(\mathbf{r}) \equiv \phi_A(\mathbf{r}) - f$, which is the deviation of the A monomer concentration from its average value. The parameters above are given by

$$\begin{aligned} f &= 1/2 \\ q_0 &\simeq 1.95/R_g; \quad \tau = 2\rho N\left(\chi_\mathrm{c} - \chi\right). \end{aligned} \quad (2)$$

With a monomer size a, the gyration radius for Gaussian chains is $R_g^2 \simeq \frac{1}{6}Na^2$, and $\rho = 1/Na^3$. Other parameters in equation (1) are

$$\chi_\mathrm{c} \simeq 10.49/N; \quad h = 3\rho c^2 R_g^2/2q_0^2. \quad (3)$$

The dimensionless parameters u/ρ and c are of order unity. The reduced temperature $\tau \sim (\chi_\mathrm{c} - \chi)$ is positive in the disordered phase, where $\phi(\mathbf{r}) = 0$. Close to the ODT the bulk system is described by two length scales: the first is the periodicity of lamellar modulations $d_0 = 2\pi/q_0$, and the second is the correlation length $\sim (\tau/h)^{-1/4}$, characterizing the decay of surface induced modulations. This length diverges at the ODT, $\chi = \chi_\mathrm{c}$.

The interaction free energy of a BCP melt with the confining wall (in units of $k_\mathrm{B}T$) can be written as a sum of two terms

$$\mathcal{F}_s = \int \left[\sigma(\mathbf{r}_s)\phi(\mathbf{r}_s) + \tau_s\phi^2(\mathbf{r}_s)\right] \mathrm{d}^2\mathbf{r}_\mathrm{s} \quad (4)$$

where $\{\mathbf{r}_s\}$ denotes the wall position. The first term is linear in the order parameter, and expresses preferential adsorption: a positive $\sigma(\mathbf{r}_s)$ induces a negative $\phi(\mathbf{r}_s)$ (preference to the B monomers). The second (quadratic) term allows surface deviation of the Flory parameter χ from its bulk value. A positive τ_s means that the surface has an ordering temperature lower than the bulk one [28].

In the following we consider a thin film in which the melt is confined by two flat and parallel walls at $y = \pm L$. Interactions between the wall and the melt are assumed to be short-range, and for homogeneous walls, $\sigma(\mathbf{r}_s) =$ const., used throughout this paper, no additional surface length scales are introduced (see Refs. [17–19,29] where $\sigma(\mathbf{r}_s)$ varies on the walls). The strength of wall interaction is given by two parameters: $\sigma^+ = \sigma(y = L)$ and $\sigma^- = \sigma(y = -L)$. Symmetric ($\sigma^+ = \sigma^-$) and asymmetric ($\sigma^+ = -\sigma^-$) walls will be considered as special cases.

The deviation of the order parameter, $\phi(\mathbf{r})$, from its bulk value $\phi_b(\mathbf{r})$ is denoted by $\delta\phi$

$$\delta\phi(\mathbf{r}) \equiv \phi(\mathbf{r}) - \phi_b(\mathbf{r}). \quad (5)$$

This deviation contains the effect of the walls. The free energy $\mathcal{F} = \mathcal{F}_b + \mathcal{F}_s$ is then expanded to second order around its bulk value, $\mathcal{F} = \mathcal{F}[\phi_b] + \Delta\mathcal{F}[\delta\phi, \phi_b]$,

$$\begin{aligned} \Delta\mathcal{F} = \int \Big\{ & [(\tau + hq_0^4)\phi_b + \frac{1}{6}u\phi_b^3 + hq_0^2\nabla^2\phi_b]\delta\phi \\ & + \frac{1}{2}(\tau + \frac{1}{2}u\phi_b^2)\left(\delta\phi\right)^2 + \frac{1}{2}h\left(\nabla^2\delta\phi + q_0^2\delta\phi\right)^2 \Big\} \mathrm{d}^3\mathbf{r} \\ & + \int \left[\sigma\delta\phi + \tau_s\left(2\phi_b\delta\phi + \delta\phi^2\right)\right] \mathrm{d}^2\mathbf{r}_\mathrm{s}. \end{aligned} \quad (6)$$

In the next section we investigate the parallel and perpendicular lamellar phases denoted as $L_\parallel$ and $L_\perp$, respectively, and choose the appropriate forms for their bulk phase ϕ_b. The free energy, equation (6), is then minimized with respect to the correction field $\delta\phi$ and yields the BCP profile.

3 Order parameter profiles

The cases of parallel $L_\parallel$ and perpendicular $L_\perp$ phases are now considered separately.

3.1 Perpendicular lamellar phase: $L_\perp$

Up to this point $\delta\phi$ and ϕ_b were not specified. For films below the ODT ($\tau < 0$), the perpendicular bulk phase $L_\perp$ has the bulk periodicity $d_0 = 2\pi/q_0$. Its order parameter is given in the single mode approximation (close to the ODT) by [30]

$$\phi_b(\mathbf{r}) = \phi_q \cos(q_0 x) \quad (7)$$

the amplitude $\phi_q = (-8\tau/u)^{1/2}$ is obtained from a variational principle of the bulk free energy.

The order parameter for the perpendicular lamellae is

$$\begin{aligned} \phi_\perp(\mathbf{r}) &= \phi_b(\mathbf{r}) + \delta\phi(\mathbf{r}) \\ \delta\phi(\mathbf{r}) &= w(y) + g(y)\cos(q_0 x) \end{aligned} \quad (8)$$

where for the correction field $\delta\phi$ we use the single mode ansatz. If additional modes are included in the bulk order parameter, equation (7), such modes should also be included in equation (8).

For the above choice of ϕ_b [Eq. (7)], it is now possible to perform the x and z integration explicitly, retaining only the y dependency in equation (6). The free energy per unit area can be written as

$$\Delta F_\perp = \Delta F_g + \Delta F_w \quad (9)$$

where

$$\begin{aligned} \Delta F_g = \int \left\{ -\frac{1}{2}\tau g^2 + \frac{1}{4}h\left(g''\right)^2 \right\} \mathrm{d}y \\ + \tau_s\phi_q(g_+ + g_-) + \frac{1}{2}\tau_s(g_-^2 + g_+^2) \end{aligned} \quad (10)$$

and

$$\Delta F_w = \int \left\{ -\frac{1}{2}\tau w^2 + \frac{1}{2}h\left(q_0^2 w + w''\right)^2 \right\} \mathrm{d}y + \sigma^- w_- + \sigma^+ w_+ + \tau_s (w_-^2 + w_+^2) \qquad (11)$$

where $g_\pm \equiv g(\pm L)$ and $w_\pm \equiv w(\pm L)$.

The amplitude function $g(y)$ results from the surface modification of the Flory parameter, $\tau_s \lessgtr 0$, and it vanishes if τ_s vanishes. This can be seen by noting that if $\tau_s = 0$ then the minimum of the integral in equation (10) is obtained for $g(y) \equiv 0$ (recalling that $\tau < 0$). There is no coupling between $w(y)$ and $g(y)$, since the free energy is expanded to second order in $\delta\phi$, and the mixed terms are of higher order. The function $w(y)$ minimizes ΔF_w subject to the condition that $\int w(y)\mathrm{d}y$ is fixed. Using λ as the Lagrange multiplier, it satisfies an ordinary fourth order differential equation

$$\left(q_0^4 - \frac{\tau}{h}\right) w(y) + 2q_0^2 w''(y) + w''''(y) - \frac{\lambda}{h} = 0. \qquad (12)$$

Similarly, the equation for $g(y)$ is

$$-\frac{2\tau}{h} g + g'''' = 0. \qquad (13)$$

A Lagrange multiplier is not needed here because $\int g(y)\cos(q_0 x)\,\mathrm{d}^3 r = 0$. These equations are linear in $w(y)$ and $g(y)$ since the free energy, equation (6), is expanded to second order around ϕ_b. The four boundary conditions for $g(y)$ are

$$2\tau_s \phi_q + 2\tau_s g_\pm \mp h g'''(\pm L) = 0 \qquad (14)$$

$$g''(\pm L) = 0 \qquad (15)$$

and for $w(y)$

$$\sigma^\pm + 2\tau_s w_\pm \mp q_0^2 h w'(\pm L) \mp h w'''(\pm L) = 0 \qquad (16)$$

$$q_0^2 w_\pm + w''(\pm L) = 0 \qquad (17)$$

$$\int_{-L}^{L} w(y)\mathrm{d}y = 0. \qquad (18)$$

Equation (18) expresses the condition that the total A/B fraction is conserved, $\int \delta\phi(\mathbf{r})\mathrm{d}^3 r = 0$.

All coefficients in equations (12) and (13) are constants, and therefore the solutions $g(y)$ and $w(y)$ have the form:

$$w(y) = A_w \mathrm{e}^{-k_w y} + B_w \mathrm{e}^{k_w y} + A_w^* \mathrm{e}^{-k_w^* y} + B_w^* \mathrm{e}^{k_w^* y} + \text{const.} \qquad (19)$$

$$g(y) = A_g \mathrm{e}^{-k_g y} + B_g \mathrm{e}^{k_g y} + A_g^* \mathrm{e}^{-k_g^* y} + B_g^* \mathrm{e}^{k_g^* y} \qquad (20)$$

where O^* denotes the complex conjugate of the variable O. The complex amplitudes A_w, B_w, A_g and B_g and the constant term in equation (19) are determined from the boundary conditions.

The complex wavevectors k_w and k_g are given by

$$k_w^2 = -q_0^2 + (\tau/h)^{1/2} \qquad (21)$$

$$k_g^2 = (2\tau/h)^{1/2}. \qquad (22)$$

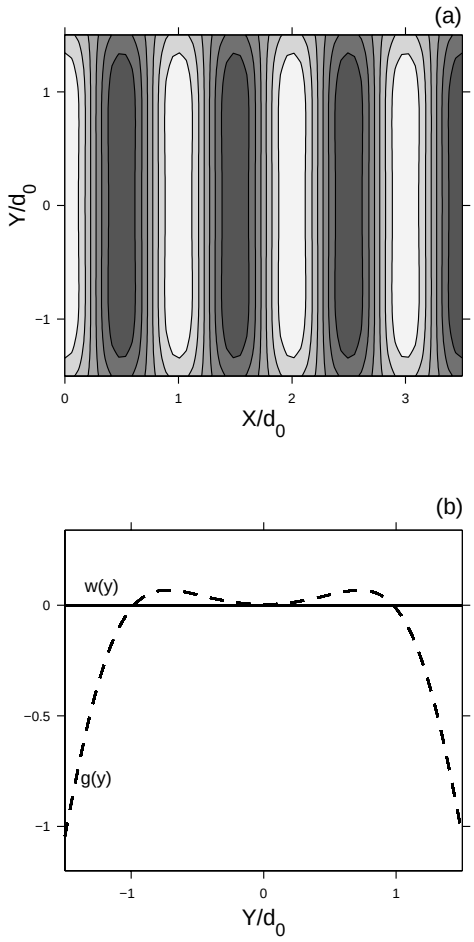

Fig. 1. Contour plot of the perpendicular lamellar phases between two homogeneous walls. The A monomers are shown in light shades while the B ones are dark. In (a) the two walls at $y = \pm L = \pm 1.5 d_0$ are neutral, $\sigma^\pm = 0$. Part (b) shows the correction fields $w(y)$ (solid line) and $g(y)$ (dashed line) in $\delta\phi(\mathbf{r}) = w(y) + g(y)\cos(q_0 x)$. A surface Flory parameter which is different from the bulk value, $\tau_s > 0$, causes surface deviations of the lamellar structure from its bulk shape, even for neutral walls. The Flory parameter is $\chi N = 10.8$, $\tau_s = 0.1 h q_0^3$. In this and subsequent figures we use $u/\rho = c = 1$ and $N = 1000$.

In the vicinity of the ODT, $\tau \approx 0$, and the real and imaginary parts of $k_w = k_w' + \mathrm{i}k_w''$ are given approximately by

$$k_w' \approx \frac{\alpha}{2q_0}\left(N\chi - N\chi_\mathrm{c}\right)^{1/2} \qquad (23)$$

$$k_w'' \approx q_0 \left(1 - \alpha^2 \frac{N\chi - N\chi_\mathrm{c}}{8q_0^4}\right) \qquad (24)$$

where $\alpha \equiv 2q_0^2/(1.95\sqrt{3}c)$ follows from equations (2) and (3). The period of modulations $2\pi/k_w''$ tends to $2\pi/q_0$, and the decay length of these modulations $\xi_w = 1/k_w'$ diverges as $\xi_w \sim (N\chi - N\chi_\mathrm{c})^{-1/2}$ in the limit $\tau \to 0$ [17,18].

A contour plot of the order parameter $\phi(x,y) = \phi_b(x,y) + \delta\phi(x,y)$ is shown in Figure 1a, for inter-plate separation $2L = 3d_0$. The two walls at $y = \pm L$ are neutral,

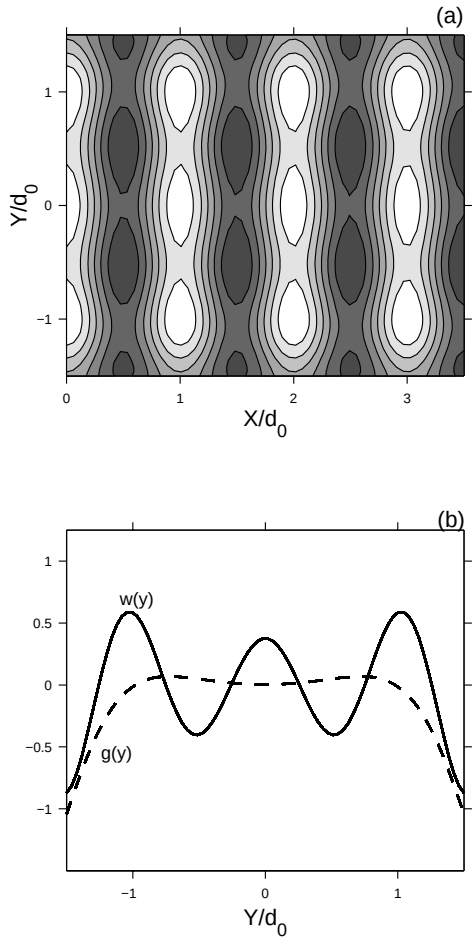

Fig. 2. Same as in Figure 1, but here the two walls favor the B monomers, $\sigma^{\pm} = 0.2hq_0^3\phi_q > 0$. Monomers are rearranged near the walls and the A/B inter-material dividing surface (IMDS) is curved (see also Fig. 3). The preferential walls induce parallel ordering, as $w(y) \neq 0$ in (b). The length scale of modulation in (a) is determined by the functions $w(y)$ and $g(y)$ in (b) [Eqs. (19) and (20)].

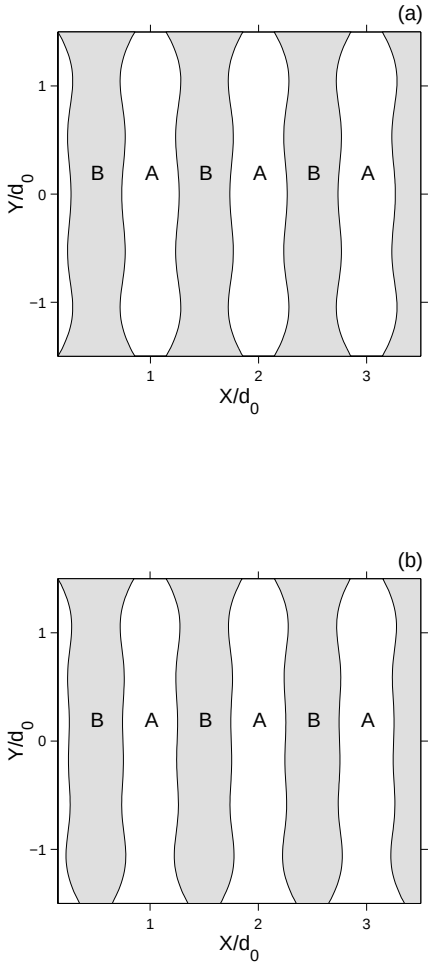

Fig. 3. Parts (a) and (b) are plots of the IMDS (defined by $\phi(\mathbf{r}) = 0$) of confined perpendicular $L_{\perp}$ lamellae. In (a), the two walls favor the B monomers, $\sigma^{\pm} = 0.2hq_0^3\phi_q > 0$, and the B domains are larger than the A domains at the walls. In (b) $\sigma^{-} = -\sigma^{+} = 0.2hq_0^3\phi_q$, and the A domains have large size at $y = -L$, while the B domains are larger at $y = L$. The Flory parameter is $N\chi = 11$ and $\tau_s = 0.1hq_0^3$.

$\sigma^{\pm} = 0$, but the surface Flory parameter deviates from its bulk value, $\tau_s > 0$. Note that the interfacial width broadens close to the wall, but the A/B inter-material dividing surface (IMDS) (defined as the surface where $\phi(x, y) = 0$) is perpendicular to the walls. This result is similar to the one obtained in reference [16] (their Fig. 3), using different methods. In Figure 1b we show the response fields $g(y)$ and $w(y)$ in $\delta\phi = w(y) + g(y)\cos(q_0 x)$. It is advantageous for the lamellae to reduce their amplitude close to the wall, hence, in our convention, a positive $\tau_s > 0$ induces a negative $g(y = 0)$. The amplitude of sinusoidal modulations in $\phi(x, y) = w(y) + (\phi_q + g(y))\cos(q_0 x)$ is therefore diminished from it unperturbed value ϕ_q. In the absence of surface fields, $\sigma^{\pm}$, the w part of $\delta\phi$ vanishes, $w(y) = 0$.

Figure 2 is similar to Figure 1, but the symmetric walls ($\sigma^{+} = \sigma^{-}$) are chosen here to favor the B monomers (in dark), which partially wet them.

As a result, the A/B IMDS bends and intersects with the walls at an angle which is different than 90°. The preferred adsorption is also seen in Figure 2b, where $w(y)$ is negative at the walls, $w_{\pm} < 0$.

The copolymer contour lines are defined by the relation $\phi(\mathbf{r}) = \phi_b(\mathbf{r}) + \delta\phi(\mathbf{r}) = c$, where c is a constant. Clearly, the inter-material dividing surface (IMDS) is just the special case with $c = 0$. For bulk lamellar phase the IMDS are just parallel planar surfaces (lines in two dimensions), but for lamellae confined in thin films the shape of these lines is more complicated. Figure 3a shows the IMDS lines for symmetric walls, both favoring the B monomer. As expected, the contact area of the B domains with the wall is increased, and the IMDS lines are curved appropriately. A different behavior is seen in Figure 3b (asymmetric walls) where the curving of the IMDS lines is opposite at the two surfaces because of the opposite wall interaction. The deviation from a perfect lamellar shape is seen as the IMDS undulates.

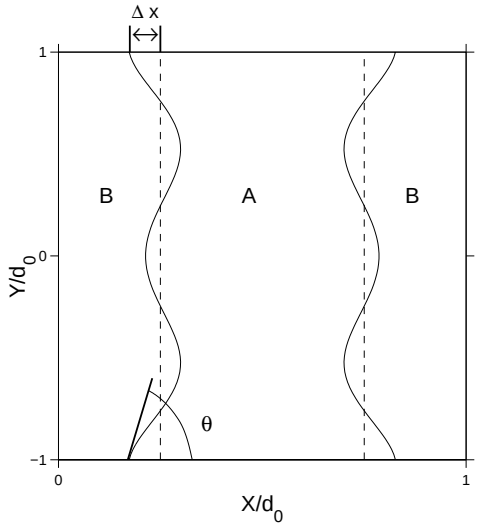

Fig. 4. Schematic drawing of the IMDS lines. The confining walls are at $y = \pm L = \pm d_0$. The dotted line is the location of the unperturbed IMDS. The lateral deviation from this line at the walls is Δx. The angle between the tangent to the IMDS and the x-axis is θ.

In general, contour lines do not run perpendicular to the wall but rather form an angle different than 90° with the surface. On contour lines having $\phi = \text{const.}$, x and y are related by

$$\cos q_0 x = \frac{c - w(y)}{\phi_q + g(y)} \cdot \tag{25}$$

Figure 4 is a schematic presentation of the IMDS. The dotted vertical line shows the unperturbed location of the A/B IMDS. At the $y = -L$ wall, the deviation Δx of the IMDS from this line (see Fig. 4) is

$$\frac{\Delta x}{d_0} = \frac{1}{2\pi} \arccos\left(\frac{-w_-}{\phi_q + g_-}\right) - \frac{1}{4} \cdot \tag{26}$$

The departure from the flat interface can be quite large, for example, in Figure 3a it is $\Delta x/d_0 \approx 0.1$. We define θ as the angle at which the IMDS line $y(x)$ joins the wall at $y = -L$. For neutral walls, $\Delta x = 0$ and $\theta = 90°$. From equation (25) it follows that

$$\tan\theta = \frac{\mathrm{d}y}{\mathrm{d}x} = \frac{q_0 \sin(q_0 \Delta x)(\phi_q + g_-)^2}{w'(-L)(\phi_q + g_-) + w_- g'(-L)} \cdot \tag{27}$$

Using the same parameters as in Figure 3a, we find that $\theta \approx 80°$.

As the ODT is approached from below ($\tau < 0$), the lamellae can be deformed more easily. The energetic cost of lamellae bending and compression is reduced, and the IMDS departs appreciably from its flat shape. The effect of temperature is clearly seen in Figure 5, where in (a) the IMDS is plotted for Flory parameter $\chi N = 12$, while in (b) the temperature is higher and closer to the ODT, $\chi N = 11$, and the contour lines show stronger undulations. Close to the ODT, the length scale associated with the undulation periodicity is $2\pi/k''_w \approx d_0$ [see Eq. (24)], but it may get much smaller as the temperature is reduced, $\chi \gg \chi_c$. The second length scale in the system, $2\pi/k'_w$, characterizes the decay of modulations, and it diverges at the ODT.

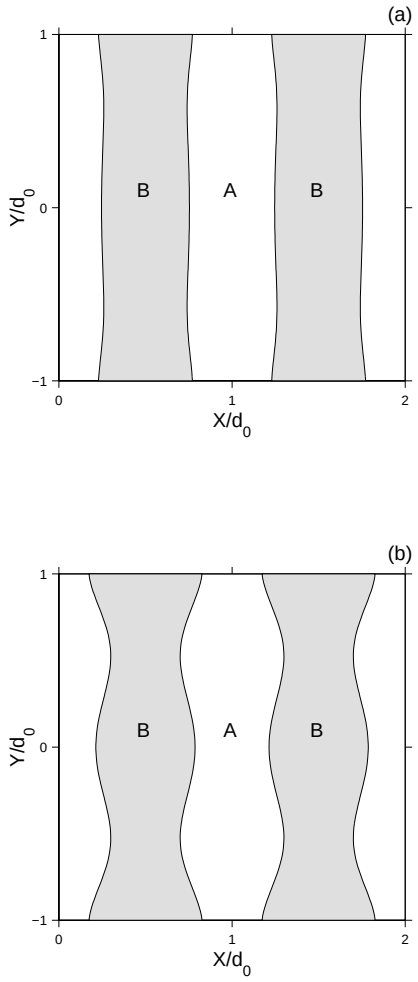

Fig. 5. Temperature dependence of the shape of the IMDS. In (a) the Flory parameter is $\chi N = 12$ (relatively strong segregation), and the IMDS are nearly flat. As the temperature is raised and approaches the ODT, $\chi N = 11$ in (b), the lamellae can easily deform in accordance with the surface fields $\sigma^{\pm}$. The shape of decaying undulations is given by equation (25) with $c = 0$. The parameters chosen are $\sigma^{\pm} = 0.5 h q_0^3$ and $\tau_s = 0$.

3.2 Parallel lamellar phase: $\mathsf{L}_{\|}$

The alternative case of lamellar order occurs when the lamellae are parallel to the walls, and the A/B profiles depend only on the distance from the walls, $\phi(\mathbf{r}) = \phi(y)$. In the strong stretching approximation [11,20], the lamellae are allowed to stretch or compress in order to vary their natural periodicity d_0 according to the constraint interplate separation $2L$. The system can have n or $n \pm 1/2$ lamellae between the walls, where n is the closest integer

to $2L/d_0$. This strong stretching calculation motivates our zeroth order approximation to the $L_\parallel$ phase,

$$\phi_b(\mathbf{r}) = \pm\phi_q \cos[q(y+L)]. \tag{28}$$

Using n from above, the wavenumber is $q = n\pi/L$ or $(n+1/2)\pi/L$. The lamellae are stretched if $q < q_0$ and compressed if $q > q_0$. The $\pm$ sign of the profile is determined by the wall interactions.

The bulk approximation for the profile, equation (28), serves as a starting point. However, the correction field, $\delta\phi$, has an important contribution in the weak segregation. The order parameter for the parallel phase $L_\parallel$ is

$$\begin{aligned}\phi_\parallel(\mathbf{r}) &= \phi_b(\mathbf{r}) + \delta\phi(\mathbf{r}) \\ \delta\phi(\mathbf{r}) &= w(y).\end{aligned} \tag{29}$$

The free energy (per unit area) has y-dependent terms only. Expanded to second order in $w(y)$, it can be written as:

$$\begin{aligned}\Delta F_\parallel = \int \left[\frac{1}{2}(\tau + \frac{1}{2}u\phi_b^2)w^2 + \frac{1}{2}h\left(q_0^2 w + w''\right)^2\right] \mathrm{d}y \\ + \sigma^- w_- + 2\tau_s\phi_b(-L)w_- + \tau_s w_-^2 \\ + \sigma^+ w_+ + 2\tau_s\phi_b(L)w_+ + \tau_s w_+^2.\end{aligned} \tag{30}$$

Similar to the treatment of the perpendicular phase in Section 3.1, this free energy is minimized to yield a linear differential equation, but with y-dependent coefficients:

$$\begin{aligned}w''''(y) + 2q_0^2 w''(y) \\ + \left[q_0^4 - \frac{\tau}{h} - \frac{\tau}{h}\cos(2qy)\right] w(y) - \frac{\lambda}{h} = 0.\end{aligned} \tag{31}$$

The conditions imposed on $w(y)$ are:

$$\begin{aligned}\sigma^\pm + 2\tau_s\phi_b(\pm L) + 2\tau_s w_\pm \\ \mp q_0^2 h w'(\pm L) \mp h w'''(\pm L) = 0\end{aligned} \tag{32}$$

$$q_0^2 w(\pm L) + w''(\pm L) = 0 \tag{33}$$

$$\int_{-L}^{L} w(y)\mathrm{d}y = 0 \tag{34}$$

where as before λ is the Lagrange multiplier and the last equation expresses the conservation of the relative A/B concentration in the film. The homogeneous solution of equation (31) has the Bloch (Floquet) form

$$w(y) = \mathrm{e}^{-ky}\sum_n a_n \mathrm{e}^{2\mathrm{i}nqy} + \mathrm{e}^{-k^* y}\sum_n a_n^* \mathrm{e}^{-2\mathrm{i}nqy}. \tag{35}$$

A recurrence relation between the coefficients $\{a_n\}$ is obtained by substituting equation (35) in equation (31). However, the recurrence relation converges only for specific values (eigenvalues) of k. If k is a valid eigenvalue, then so are k^*, $-k$ and $-k^*$. These four eigenvalues correspond to the four independent solutions of the fourth order differential equation, equation (31).

A useful approximation to the free energy equation (30) is obtained by replacing ϕ_b^2 by its average, smeared value $\langle\phi_b^2\rangle$. This is equivalent to replace the potential term $-(\tau/h)\cos 2qy$ in equation (31) by its zero average. The governing equation for the correction field $w(y)$ is then given by a linear differential equation with constant coefficients

$$w''''(y) + 2q_0^2 w''(y) + (q_0^4 - \tau/h)w(y) - \lambda/h = 0. \tag{36}$$

Under this approximation, the form of $w(y)$ in the parallel $L_\parallel$ phase is the same as it is in the perpendicular $L_\perp$ phase, equation (19), only the boundary conditions are different.

Order parameter profiles are presented in Figure 6. The dotted line is ϕ_b as obtained by the bulk approximation, equation (28), and the solid line is the full profile, $\phi = \phi_b(y) + \delta\phi(y)$. In Figure 6a the interfacial interactions are the same on both walls, $\sigma^+ = \sigma^-$, inducing a symmetric lamellar ordering. The difference between the two curves is the correction field $\delta\phi(y)$, favoring adsorption

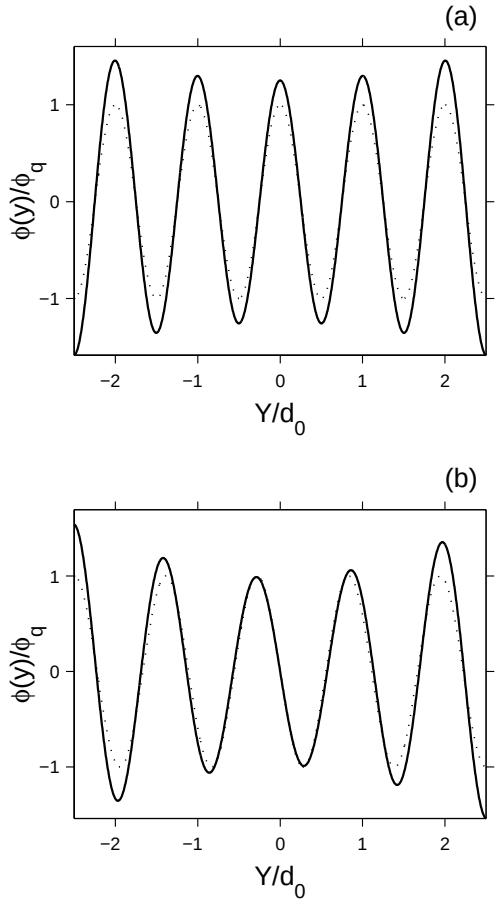

Fig. 6. Concentration profiles for the confined parallel $L_\parallel$ phase. Dotted line [$\phi = \phi_b(y)$] and solid line [$\phi = \phi_b(y) + \delta\phi(y)$] are normalized by ϕ_q. In (a) the two walls favor the B monomers ($\phi < 0$), $\sigma^\pm = 0.5hq_0^3\phi_q > 0$ and the film is symmetric, while in (b) the film is asymmetric, $\sigma^- = -\sigma^+ = -0.5hq_0^3\phi_q$, and the A monomers are adsorbed at the $y = -L$ wall. The bulk Flory parameter is $\chi N = 10.6$ and its surface modification is $\tau_s = 0.125hq_0^3$.

of the B monomers ($\phi < 0$) at the two walls. In Figure 6b the film is asymmetric with $\sigma^+ = -\sigma^-$, and adsorption of the A monomers at the $y = -L$ wall is enhanced.

4 Free energy and stability diagram

Once the order parameter profiles for the parallel and perpendicular lamellar phases are calculated, the corresponding free energies can be evaluated by substituting the order parameter profiles in equations (30) and (9), respectively. The reference free energy $F^0[\phi_b]$ is calculated by the bulk approximation. For the parallel lamellae it is given by substituting the profile, equation (28), directly into equation (1),

$$F^0_{\parallel}[\phi_b] = \left[\frac{1}{4}\tau\phi_q^2 + \frac{1}{4}h(q_0^2 - q^2)^2\phi_q^2 + \frac{u}{64}\phi_q^4\right] 2L \pm \sigma^-\phi_q \pm \sigma^+\phi_q + 2\tau_s\phi_q^2 \quad (37)$$

where the $\pm\sigma$ terms result from the choice of the bulk order parameter ϕ_b. For the perpendicular phase $L_\perp$, substituting the profile, equation (7), results in:

$$F^0_{\perp}[\phi_b] = \left[\frac{1}{4}\tau\phi_q^2 + \frac{u}{64}\phi_q^4\right] 2L + \tau_s\phi_q^2 = -\frac{2L\tau^2}{u} + \tau_s\left(\frac{-8\tau}{u}\right) \quad (38)$$

As a function of inter-plate separation $2L$, the total free energy $F[\phi_b + \delta\phi]$ has oscillations, as depicted in Figure 7 for symmetric film, $\sigma^- = \sigma^+$. The free energies of the perpendicular and parallel lamellar phases (solid line and thick solid line, equations (9) and (30), are lower than the bulk ones $F^0_{\parallel}[\phi_b]$ and $F^0_{\perp}[\phi_b]$ (dotted and dashed lines). In Figure 7a the wall interactions are $\sigma^{\pm} = 0.4hq_0^3\phi_q$, and the free energy of the $L_\parallel$ phase is slightly reduced from the bulk approximation value. Additional minimum develops at $2L \approx 1.5d_0$. The $L_\perp$ free energy has a marked minimum for $2L \lesssim d_0$ [14], see inset. In Figure 7b the interfacial interactions are smaller, $\sigma^{\pm} = 0.2hq_0^3\phi_q$, and in this case the $L_\parallel$ free energy is notably lowered from the bulk approximation calculation. However, the difference between the two curves tends to zero as $2L/d_0 \to \infty$, because the surface induced modulations have finite range. For both choices of σ, the $L_\perp$ free energy is significantly lowered from its bulk approximation value. Note that the bulk approximation curves are similar to the curves obtained in the strong stretching approximation.

Restricting ourselves to $L_\parallel$ and $L_\perp$ lamellar phases, the stability diagram is constructed as a function of two system parameters: the inter-wall separation $2L$ and the surface preference $\sigma^{\pm}$. In the first stage, we ignore the correction presented above, and use $F^0_{\parallel}[\phi_b]$ and $F^0_{\perp}[\phi_b]$ as given by the bulk approximation calculation. The stability diagram in Figure 8 is calculated for walls having a fixed ratio of surface interaction $\sigma^+ = -2\sigma^-$. Parallel lamellae at $2L/d_0 = n$, for integer n, have symmetric ordering, while antisymmetric ordering occurs for $2L/d_0 = n + 1/2$.

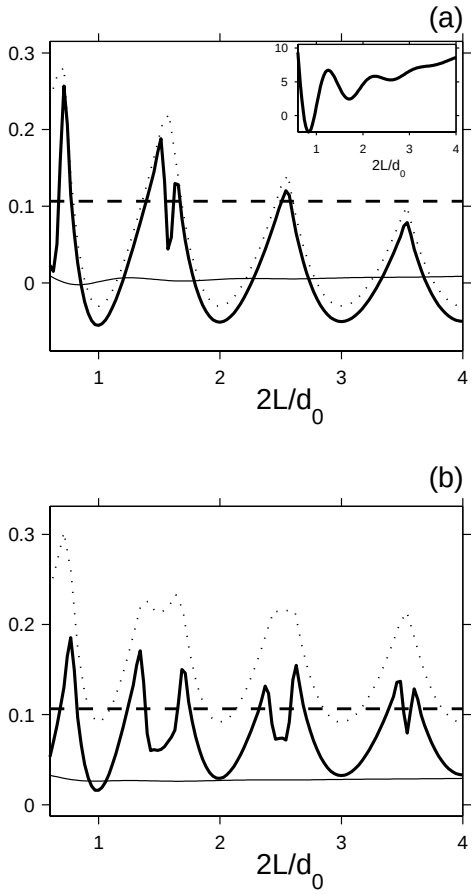

Fig. 7. Film free energy per unit area as a function of inter-plate separation $2L$. Shown are the bulk approximation to the free energy of the $L_\perp$ phase (horizontal dashed line), bulk approximation of $L_\parallel$ (dotted line), full free energy of the $L_\perp$ (solid line) and of the $L_\parallel$ phase (thick solid line). The film is taken to be symmetric. In (a) $\sigma^{\pm} = 0.4hq_0^3\phi_q$, while in (b) the surface interactions are smaller, $\sigma^{\pm} = 0.2hq_0^3\phi_q$. Free energies are measured with respect to the free energy of the bulk lamellar phase. Inset in (a) is an enlargement of the $L_\perp$ free energy by a factor of 10^3, showing a deep minimum for $2L \lesssim d_0$. The bulk Flory parameter is $\chi N = 11$ and its surface deviation is $\tau_s = 0.35hq_0^3$.

The difference in the diagram is caused by the choice of σ's. In Figure 8a the surface Flory parameter is the same as the bulk one, $\tau_s = 0$. For neutral walls, $\sigma^{\pm} = 0$, the perpendicular lamellae (in dark) are stable. A degeneracy between $L_\perp$ and $L_\parallel$ phases occurs for $2L/d_0 = n$ or $n + \frac{1}{2}$ ($n = 0, 1, 2 \ldots$), where the parallel lamellae are not frustrated and $q = q_0$. The parallel lamellae (in light color) are preferred if the surface interaction is strong enough to overcome the lamellar stretching or compression. The use of a weak segregation bulk approximation agrees with previously obtained stability diagrams in intermediate and strong segregations [15,16].

In Figure 8b we present the bulk approximation, but now the surface Flory parameter is changed, $\tau_s = 0.1hq_0^3 > 0$. The $L_\parallel$ phase is pushed upward and the

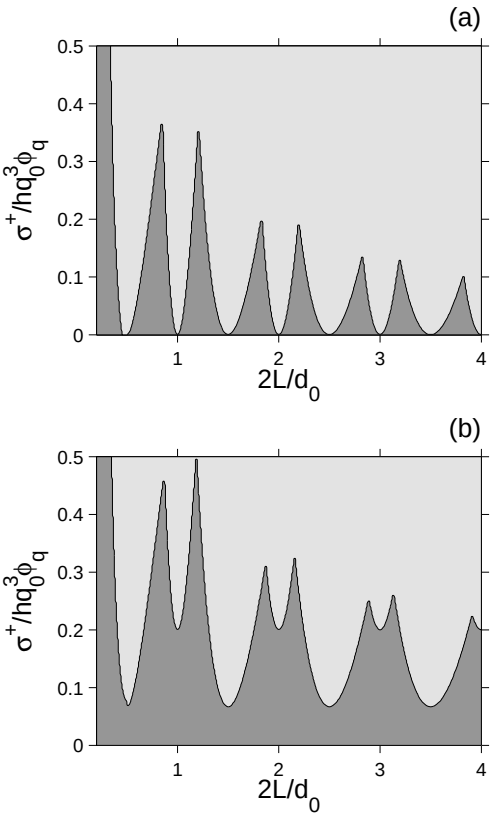

Fig. 8. The stability of $L_\parallel$ (in light) *vs.* $L_\perp$ lamellae (in dark), as a function of wall separation $2L$ and interfacial strength σ^+. The free energies are taken from equations (37) and (38), respectively. In (a) the surface Flory parameter is the bulk one, $\tau_s = 0$, while in (b) $\tau_s = 0.1hq_0^3 > 0$. The $L_\parallel$ phase is pushed upward in the stability diagram in (b), removing the degeneracy between $L_\perp$ and $L_\parallel$ that occurs for neutral walls ($\sigma^\pm = 0$) when $\tau_s = 0$. The calculation is done by the bulk approximation, $\phi(\mathbf{r}) = \phi_b(\mathbf{r})$. The ratio $\sigma^+/\sigma^- = -2$ is kept constant and the Flory parameter is $\chi N = 11$.

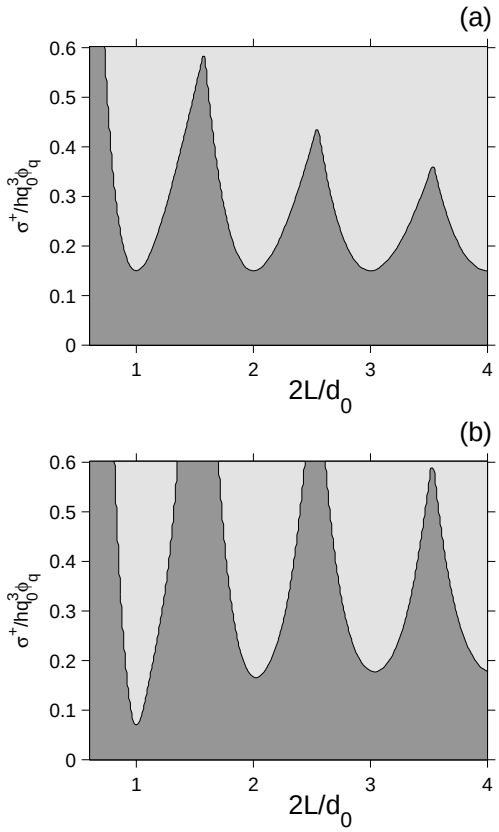

Fig. 9. Stability of $L_\parallel$ (in light) *vs.* $L_\perp$ lamellae (in dark), comparing in (a) the bulk approximation [free energy Eqs. (37) and (38)], with the full free energy in (b) (calculated from Eq. (1) with Eqs. (29) and (8), respectively). Note that the large σ^+ behavior lies outside the range of validity of our linear model. In both parts (a) and (b) $\tau_s = 0.3hq_0^3$, the Flory parameter is $\chi N = 10.8$ and the film is symmetric, $\sigma^- = \sigma^+$.

diagram is different. Symmetric phases ($2L \approx nd_0$) are pushed more than the asymmetric ones ($2L \approx (n + \frac{1}{2})d_0$) because of our choice of surface fields σ's. In the bulk approximation, the free energy of unfrustrated parallel lamellae [$q = q_0$ in Eq. (37)] is higher than that of the perpendicular lamellae [Eq. (38)] if the walls are neutral. As a result, the $L_\perp$ morphology is favored for all separations $2L$, and the degeneracy is removed [15,16]. Clearly, a surface segregation temperature different than the bulk one ($\tau_s \neq 0$) can account for the experimental lack of this degeneracy [31]. According to the same reasoning, if $\tau_s < 0$ then the parallel phases are preferred on the expense of the $L_\perp$ phases, and, in particular, for wall separations $2L \approx nd_0$. Note that the last sentence agrees with the different dependence on τ_s seen in equations (37) and (38). For parallel lamellae, the surface term is $2\tau_s\phi_q^2$, while for perpendicular lamellae it is only $\tau_s\phi_q^2$.

Figure 9 shows the stability diagram, where in (a) we use the bulk approximation for symmetric $\sigma^- = \sigma^+$ film, and in (b) we used the full, and correct, order parameter $\phi = \phi_b + \delta\phi$. The parallel ordering is then always symmetric. A general feature of this diagram is that the $L_\perp$ phase is more stable relative to the $L_\parallel$ for larger surface fields for $2L > d_0$. The figure also demonstrates the qualitative agreement with the bulk approximation.

5 Conclusions

We have used a Ginzburg-Landau free energy to study analytically the thin-film ordering of diblock copolymers (BCP) in the weak segregation regime. The two homogeneous confining walls are assumed to have short-range interactions with the BCP blocks. The free energy is expanded to second order around the appropriately chosen bulk phase, and the correction field $\delta\phi$ is obtained. The use of such free energy formulation is advantageous because it offers simple analytical results and complements numerical studies. However, our mean-field approach is limited to a region of temperatures in the vicinity of the ODT, but not too close to it, where critical fluctuations

are known to be important [5]. Very close to the ODT, the response field $\delta\phi$ diverges. However, if the surface Flory parameter is different from the bulk one, $\tau_s > 0$, the surface has a lower ordering temperature than the bulk, and this divergence is absent [32].

For confined parallel $L_\parallel$ and perpendicular $L_\perp$ phases, the correction field $\delta\phi$ adds an enrichment layer of the preferred component, with thickness $\xi \sim 1/k\omega'$ diverging at the ODT. This thickness is obtained as a special case for patterned walls (inhomogeneous σ) studied by us before. Effects of finite chain length, however, preclude the divergence of this thickness. In the $L_\perp$ phase, an increase of the surface fields $\sigma^\pm$ increases the correction field $\delta\phi$, and induces a parallel lamellar ordering until, eventually, there is no clear distinction between $L_\parallel$ and $L_\perp$.

In general, the IMDS lines are bent and deviate from their flat shape in bulk lamellar system. Previous works used a phenomenological model valid in the strong segregation regime, and obtained a linear equation for the deviation of the IMDS. The resulting order parameter expressions for the confined phases are crude, when compared to Monte-Carlo simulations [22–24]. In the weak segregation presented here, the order parameter itself is linearized. Using the expressions given above for $\phi_b(\mathbf{r})$ and $\delta\phi(\mathbf{r})$, one can deduce the shape of an arbitrary equi-ϕ line given by $\phi(\mathbf{r}) = c$. We give expressions for the angle of the IMDS with the confining walls, and the deviation of the IMDS from its flat shape. This deviation, characterized by decaying oscillations, can be quite large and can even reach $20\% - 30\%$ of the lamellar width d_0. We note that in an experimental setup whose target is to produce perpendicular lamellae, system parameters should be tuned in order to keep the lamellae as flat and parallel as possible.

The free energy as a function of wall separation $2L$ is different from the bulk approximation. The free energy of the $L_\perp$ phase is lower than the one obtained the bulk approximation, as is seen in Figure 7a. The curve has decaying oscillations and tends to a constant when $2L \gg d_0$. The correction to the $L_\parallel$ free energy has similar undulatory character and under different conditions its effect can be large, as in Figure 7b. The pressure, $-\partial F/\partial y$, is different than what is expected from the bulk approximation, since additional maxima and minima are present in the free energy. Our bulk approximation yields order parameter and energy profiles which are the same (apart from numerical values) as those obtained by the strong stretching theory of Walton *et al.* and Turner [11,20].

In experiment with neutral walls, perpendicular lamellae are always favored over unfrustrated parallel lamellae (of period d_0) [31], in contrast to the common strong stretching prediction [11,15,20]. We first compute the bulk stability diagram and find it similar to previous intermediate and strong segregation calculations [15,16]. We then show that proper account of the surface change of the Flory parameter ($\tau_s > 0$) can explain the experimental findings, and significantly change the stability diagram (compare Fig. 8a to 8b). Thus, perpendicular lamellae are expected to have the lowest free energy at all separations $2L$, as in Figure 8b. We point out that if the surface ordering temperature is higher than the bulk ODT temperature, *i.e.* $\tau_s < 0$, the $L_\parallel$ phase may become stable even for neutral walls at $2L = nd_0$. However, this is yet to be confirmed experimentally.

The stability diagram in this paper is similar to the diagram in [15]. For symmetric walls, $\sigma^+ = \sigma^-$, the $L_\perp$ is found to be stable for larger σ fields than the bulk approximation predicts, while for $2L \approx d_0$ it is stable for smaller σ fields.

One possible way to refine the calculation presented here is to use a more accurate ansatz for the bulk order parameter $\phi_b(\mathbf{r})$. Such ansatz will include more q-modes or an amplitude other than ϕ_q, further lowering the free energy.

We would like to thank M. Schick for discussions and comments. Partial support from the US-Israel Binational Foundation (B.S.F.) under grant No. 98-00429 and the Israel Science Foundation founded by the Israel Academy of Sciences and Humanities – centers of Excellence Program is gratefully acknowledged.

References

1. F.S. Bates, G.H. Fredrickson, Annu. Rev. Phys. Chem. **41**, 525 (1990).
2. T. Ohta, K. Kawasaki, Macromolecules **19**, 2621 (1986).
3. M.W. Matsen, M. Schick, Phys. Rev. Lett. **72**, 2660 (1994).
4. M.W. Matsen, F.S. Bates, Macromolecules **29**, 7641 (1996).
5. A.N. Semenov, Sov. Phys. JETP **61**, 733 (1985).
6. L. Leibler, Macromolecules **13**, 1602 (1980).
7. G.H. Fredrickson, E. Helfand, J. Chem. Phys. **87**, 697 (1987).
8. P. Lambooy, T.P. Russell, G.J. Kellogg, A.M. Mays, P.D. Gallagher, S.K. Satija, Phys. Rev. Lett. **72**, 2899 (1994).
9. G.J. Kellogg, D.G. Walton, A.M. Mayes, P. Lambooy, T.P. Russell, P.D. Gallagher, S.K. Satija, Phys. Rev. Lett. **76**, 2503 (1996).
10. P. Mansky, T.P. Russell, C.J. Hawker, J. Mayes, D.C. Cook, S.K. Satija, Phys. Rev. Lett. **79**, 237 (1997).
11. D.G. Walton, G.J. Kellogg, A.M. Mayes, P. Lambooy, T.P. Russell, Macromolecules **27**, 6225 (1994).
12. G.H. Fredrickson, Macromolecules **20**, 2535 (1987).
13. S.T. Milner, D.C. Morse, Phys. Rev. E **54**, 3793 (1996).
14. G.T. Pickett, A.C. Balazs, Macromolecules **30**, 3097 (1997).
15. M.W. Matsen, J. Chem. Phys. **106**, 7781 (1997).
16. T. Geisinger, M. Mueller, K. Binder, J. Chem. Phys. **111**, 5241 (1999).
17. Y. Tsori, D. Andelman, Macromolecules **34**, 2719 (2001).
18. Y. Tsori, D. Andelman, Europhys. Lett. **53**, 722 (2001).
19. Y. Tsori, D. Andelman, J. Chem. Phys. **115**, 1970 (2001).
20. M.S. Turner, Phys. Rev. Lett. **69**, 1788 (1992).
21. M. Park, C. Harrison, P.M. Chaikin, R.A. Register, D.H. Adamson, Science **276**, 5317 (1997).

22. Q. Wang, Q. Yan, P.F. Nealey, J.J. de Pablo, J. Chem. Phys. **112**, 450 (2000); Q. Wang, S.K. Nath, M. Graham, P.F. Nealey, J.J. de Pablo, J. Chem. Phys. **112**, 9996 (2000).
23. G.G. Pereira, D.R.M. Williams, Macromolecules **31**, 5904 (1998); G.G. Pereira, D.R.M. Williams, Macromolecules **32**, 758 (1999).
24. G.G. Pereira, D.R.M. Williams, Phys. Rev. Lett. **80**, 2849 (1998).
25. K. Binder, H.L. Frisch, S. Stepanow, J. Phys. II France **7**, 1353 (1997).
26. J. Swift, P.C. Hohenberg, Phys. Rev. A **15**, 319 (1977).
27. H. Chen, A. Chakrabarti, J. Chem. Phys. **108**, 16 (1998).
28. M. Schick, in *Liquid at Interfaces, Les Houches 1988 session XLVIII*, edited by J. Charvolin, J.-F. Joanny, J. Zinn-Justin (North-Holland, Amsterdam, 1990), p. 415.
29. D. Petera, M. Muthukumar, J. Chem. Phys. **107**, 9640 (1997).
30. R.R. Netz, D. Andelman, M. Schick, Phys. Rev. Lett. **79**, 1058 (1997).
31. E. Huang, T.P. Russell, C. Harrison, P.M. Chaikin, R.A. Register, C.J. Hawker, J. Mays, Macromolecules **31**, 7641 (1998).
32. For a BCP at $y > 0$ confined by a surface at $y = 0$ with a uniform interaction parameter σ, the correction field $w(y)$ is $w(y) = A_w \mathrm{e}^{-k_w y} + \mathrm{c.c.}$ The solution of equation (12) subject to boundary conditions analogous to equations (16), (17) and (18) then gives the amplitude $A_w = -\sigma k_w (4\mathrm{i}\tau_s k_w'' + 2\mathrm{i}q_0^2(-\tau/h)^{-1/2})^{-1}$, which diverges at the ODT unless $\tau_s \neq 0$.